Supplementary Materials: Oncogenic cells evade cell competition and evolve into tumors through clone size-dependent, progressive elevation of Yki activity

Sai Katayama[1#], Seiya Nishikawa[2#], Shizue Ohsawa[3*], Atsuko Takamatsu[4*] and Tatsushi Igaki[1*]

[1]Laboratory of Genetics, Graduate School of Biostudies, Kyoto University, Yoshida-Konoecho, Sakyo-ku, Kyoto 606-8501, Japan
[2]Center for Living Systems Information Science, Graduate School of Biostudies, Kyoto University, Toshidakonoe-cho, Sakyo-ku, Kyoto 606-8501, Japan
[3]Group of Genetics, Division of Biological Science, Graduate School of Science, Nagoya University, Furo-cho, Chikusa-ku, Nagoya, Aichi, 464-8602, Japan
[4]Department of Electrical Engineering and Bioscience, Waseda University, Shinjuku-ku, Tokyo 169-8555, Japan
[1]These authors contributed equally to this work.
[*]To whom correspondence should be addressed.

S1 Deterministic model for cell competition

First, the deterministic version of mathematical model for cell competition, proposed in our previous work, is introduced [1], then it is modified for the experimental system of the main text. This model describes cell-population dynamics of two cell species, composing a monolayer tissue like an epithelial tissue. The two groups of cells, X and Y, representing normal cells (wild type cell; WT cell) and mutant cells, respectively, compete a limited resource, e.g., a space. Additionally, 'cell competition' effect at the border is considered. The equations for growth speeds of the two populations of X and Y, i.e., the number of cells, x and y can be written as follows, when X-cells encircles Y-cells as shown in Fig.S1A and B:

$$\begin{aligned} \frac{dx}{dt} &= r_x \left(1 - \frac{x+y}{K_x}\right) x \equiv f(x,y), \\ \frac{dy}{dt} &= r_y \left(1 - \frac{y+x}{K_y}\right) y - b_y y^{\frac{D}{2}} \equiv g(x,y). \end{aligned} \tag{S1}$$

The first terms of right hand side of the equations represent logistic type growth of cell population [2], where population exponentially grows first and saturates later. The exponential growth is due to initial cell proliferation, whose rate, r_x or r_y, is proportionality constant with x or y, respectively. The growth speed, however, is limited by carrying capacities, K_x or K_y, representing the final tissue size when the tissue is composed of single cell species of X or Y, respectively. Thus when Y is potentially tumorigenic, the condition $K_x < K_y$ should be applied.

The last term of right hand side of y-equation represents cell-competition effect, where X cells at the border eliminate adjacent Y cells. The strength of the elimination effect is represented by coefficient b_y. The number of adjacent Y-cells is proportional to the length of the border, which is proportional to $y^{D/2}$. The parameter D is a measure of border shape, like fractal dimension (for detailed information, see our previous work [1]). When the border shape is intricate, $1 < D < 2$ (Fig.S1A). When it is an ideal circle, $D = 1$ (Fig.S1B).

The exampled system shown in Fig.S1C have two stable fixed points S_1 and S_2, an unstable saddle fixed point S_2, and the other unstable fixed points Q_1 and S_0 around the origin, when the conditions $Kx < Ky$ and $by > 0$ are satisfied. This feature of the system results in two distinct solutions, whether cell-group X to be winner or loser. The former solution converges to $S_1(K_x,0)$, when the initial value of y is relatively small to x (the trajectory denoted with **a**). Then, cell group X become winner. The latter solution converges to Q_2, when the initial value of y is relatively large to x (the trajectory denoted with **b**). Then, cell group Y become winner. There is a separatrix discriminating the fate of the system, approximated with the line Q_1–S_2. This feature depends on shape and position of the nullcline $g(x, y) = 0$, which is controlled by parameters b_y, K_y, and D (See the reference [1] for the detail). The parameter D controls mainly the position of the nullcline $g(x, y) = 0$ in the phase-plane as shown in Fig.S1D. The parameter D larger than 1, meaning intricate border shape, acts beneficially on X-cells to be winner (nulclines **d** and **e** in Fig.S1D). This effect is similar to that of the elimination coefficient b_y, therefore, the condition $D = 1$ (nulcline **a** in Fig.S1C) is applied for simplicity in this paper hereafter and the main text.

To model the experimental system described in the main text, where various sizes of *scribble* knockdown clones were initially introduced into WT imaginal wing disk of *Drosophila*, the above equation was modified as follows considering two assumptions:

$$\begin{aligned}
\frac{dx}{dt} = f(x,y) &\equiv \begin{cases} r_x\left(1-\frac{x+y}{K_x}\right)x, & 0 < x+y \le K_x, \\ 0, & x+y > K_x, \end{cases} \\
\frac{dy}{dt} = g(x,y) &\equiv \begin{cases} r_y\left(1-\frac{y+x}{K_y}\right)y - b_y y^{\frac{D}{2}}, & y \le x, \\ r_y\left(1-\frac{y+x}{K_y}\right)y - b_y x^{\frac{D}{2}}, & y > x. \end{cases}
\end{aligned} \tag{S2}$$

The first assumption is incorporated in the equation x: Once the tissue size $x + y$ is

achieved to the normal tissue size K_x, the system of X is arrested and the X-domain size does not change anymore. This is supported by the experimental observations in which cell death in WT domain was rarely observed during the developmental process. The examples are found in our system and another system of *Rab*5-defective mutant clone [3].

The second assumption is incorporated in the equation y: The experimental system is, indeed, composed of a number of Y-clone domains. Therefore, the original model should be modified as follows. When sizes of clone domains are small enough so that X-cell group is able to encircle each Y-cell clone completely the same form as the original equation (S 1) can be used. On the contrary, when sizes of clone domains are so large that they merge each other, which was frequently observed in the system with longer period of heat-shock (see Fig. 1 in the main text), X-cell group is no longer able to encircle the Y-cell clones completely. Finally the stands of cell groups X and Y are reversed so that Y-cells encircle X-cell domain. Then the border length becomes proportional to $x^{\frac{D}{2}}$. Introducing conditions of the merging effect in precise is elaborate. Thus we simply assumed that X-cells encircles Y-cells when $y \leq x$, and Y-cells encircles X-cells when $y > x$.

The theoretical prediction by Eq.(S 2) is shown in Fig. 2. The system have a stable fixed point S_1, a line of stable fixed points L connecting to a stable fixed point Q_2 (upper part of $g(x, y) = 0$ above S_2, denoted by a thick gray curve), an unstable fixed point S_2, and the other unstable fixed points S_0 and Q_1 around the origin, in the domain of $x \geq 0$ and $y \geq 0$. This system fundamentally exhibits similar behavior to the original system of Eq. (S 1). When the initial value of y is relatively small to x (the threshold will be defined in the following paragraph), a solution converges to S_1 as shown by the curve **a**. The difference from the original system is found in the second type solution converging to a point on the line of L as shown by the curves **b**–**d**. It is observed when the initial value of y is relatively large to x. Then, Y-cell is not able to be eliminated completely. The gray dashed line $Q_1(\approx (0, 0))$-$S_2(x_{S2}, y_{S2})$ is an approximation of the separatrix discriminating the fate of the system. Examples of time evolutions of x and y are presented in Fig. S3 comparing with the result of the stochastic model introducing in the following section S2.

The threshold ratio of y to tissue size $x + y$ to determining win/lose fate is calculated as follows. The equation of the approximated separatrix is:

$$y = \frac{y_{S2}}{x_{S2}} x,$$

where

$$x_{S2} = K_x - y_{S2},$$
$$y_{S2} = \left(\frac{b_y}{r_y} \cdot \frac{1}{1 - K_y/K_x} \right)^2,$$

according to our previous work (see Supplementary Materials of section S2 in the reference [1]). Using these equations, the threshold ratio is calculated as follows:

$$\frac{y}{x + y} = \frac{y_{S2}}{K_x}. \tag{S3}$$

The value, for example, is estimated as 17 % using the parameter values of Fig. S2.

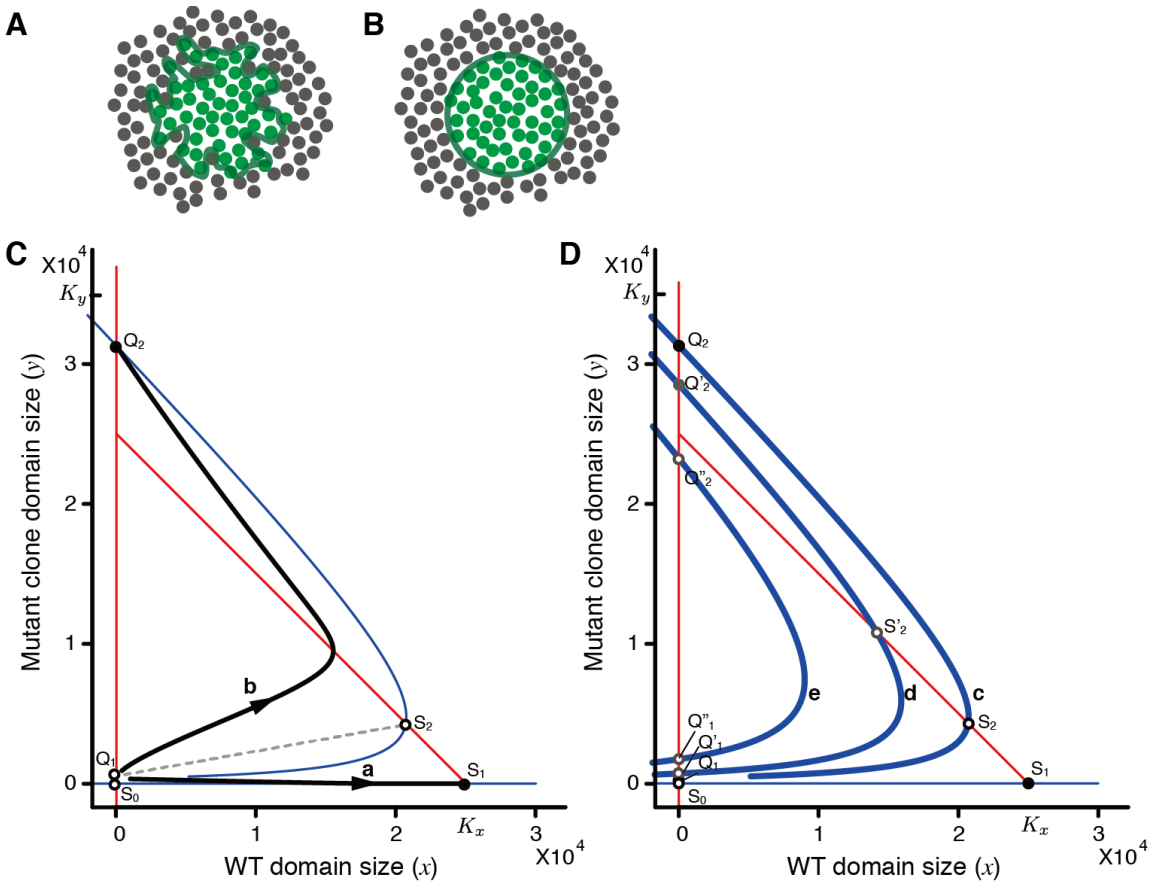

Figure S1: Cell competition effect at the border. A and B: Conceptual diagram. Green and gray closed circles represent mutant and WT cells, respectively. The border shape is intricate ($1 < D < 2$) in A, and an ideal circle in B ($D = 1$). C: Phase portrait of Eq. (S1). Red and blue solid lines are nullclines of $f(x, y) = 0$ and $g(x, y) = 0$, respectively. D: Phase portrait of Eq. (S1) with different values of D. Blue curves with notation **c**, **d**, and **e** denote the nullclines of $g(x, y) = 0$ when $D = 1$, 1.1, and 1.2, respectively. Open and closed circles represent unstable (S_2 or S'_2, Q''_2 and fixed points around the origin) and stable fixed points (S_1, and Q_2 or Q'_2), respectively. The parameters were $r_x = r_y = 0.08$ [hr^{-1}], $K_x = 25000$ [cells], $K_y = 35000$ [cells], and $b_y = 1.5$ [hr^{-1}].

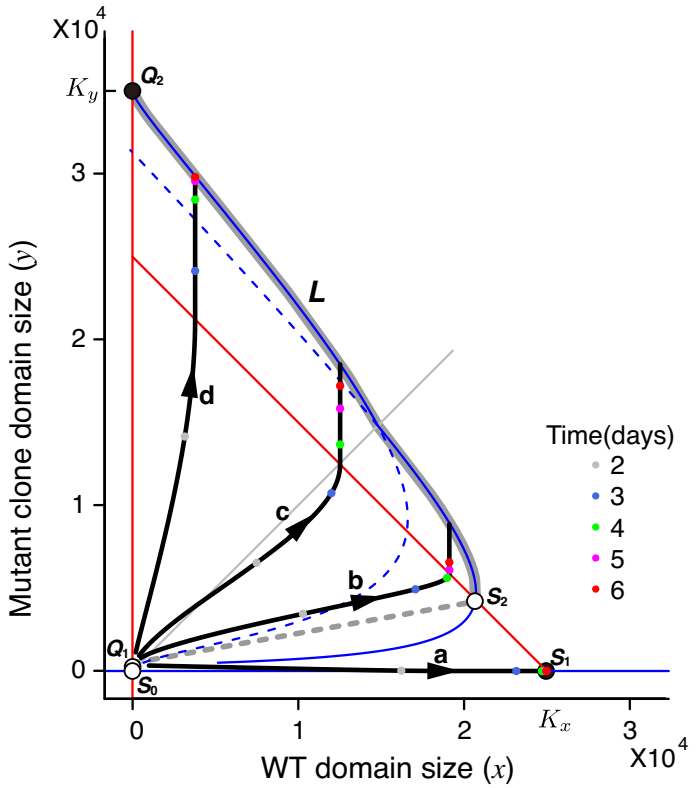

Figure S2: Theoretical prediction based on the deterministic model of cell competition, Eq. (S2). The parameters were $r_x = r_y = 0.08$ [hr^{-1}], $K_x = 25000$ [cells], $K_y = 35000$ [cells], $D = 1$, and $b_y = 1.5$ [hr^{-1}]. Blue solid curves are the nullcline of $g(x, y) = 0$, which switches on the line $x = y$ denoted by a gray thin line. Blue dashed curves are extensions of blue solid curves in the domains of $y \leq x$ and $y > x$. The black solid curves denoted with **a**–**d** are the solutions starting from at a point $(x_0, y_0) = (30, 0)$ at time $t = -2$ (d ACI), and various magnitude of heat-shocks were applied at time $t = 0$ (d ACI). The magnitudes of heat-shock were hs= 0.25, 0.60, 0.70, and 0.85, respectively, whose effects were converted into ratios of y to x at the time $t = 0$. Namely, the values of x and y were replaced into $(x, y) = ((1\text{-hs})\cdot x(t = 0), \text{hs}\cdot x(t = 0))$.

S2 Stochastic model for cell competition

The theoretical prediction by the deterministic model Eq. (S2) provides a unique solution if an initial condition is given. The experimental system, however, exhibits scattered results as seen in Fig. 1 in the main text. This can be due to stochastic effects in the system, resulted from stochasticity in cell devision and cell death, deviation in magnitude of heat-shock application, and variation in target tissue sizes. In this section, the effect of stochastic cell division is considered then the effect of the other variations are introduced.

S2.1 Stochastic process of cell division and cell death

The discrete version of the deterministic model Eq. (S2) is defined as follows:

$$\begin{aligned} x(t+\Delta t) &= x(t) + \mu_x \Delta t \cdot x(t), \\ y(t+\Delta t) &= \begin{cases} y(t) + \mu_y \Delta t \cdot y(t) - b_y \Delta t \cdot y(t)^{\frac{D}{2}}, & y(t) \le x(t), \\ y(t) + \mu_y \Delta t \cdot y(t) - b_y \Delta t \cdot x(t)^{\frac{D}{2}}, & y(t) > x(t), \end{cases} \end{aligned} \tag{S4}$$

where Δt is time interval and the parameters μ_x and μ_y are defined as follows:

$$\begin{aligned} \mu_x &= \begin{cases} r_x \left(1 - \frac{x(t)+y(t)}{K_x}\right), & 0 < x(t) + y(t) \le K_x, \\ 0, & x(t) + y(t) > K_x, \end{cases} \\ \mu_y &= r_y \left(1 - \frac{y(t)+x(t)}{K_y}\right). \end{aligned} \tag{S5}$$

This system is equivalent to a birth-death process, where μ_x and μ_y can be read as the cell-division rate of individual X- and Y-cells, respectively; and b_y can be read as the death-rate of individual Y-cells at the border. The rates μ_x and μ_y depend on the tissue size $x(t) + y(t)$ at time t as described above.

To compare with the experimental results, simulations for the birth-death process using Monte Carlo methods were performed. Simply, Poisson process was assumed for the birth and death events. Initially only X-cells, whose number is $x_0 = 30$, were prepared at time $t = -48$ [hr] (-2 [d ACI]), corresponding to the time of egg-laying. Until $t = 0$ [hr], only X-cells divide with the probability $\mu_x \Delta t$ at any time step, where $\Delta t = 0.01$ [hr] and the other parameters are presented in the figure legend of Fig. S2. At time $t = 0$ [hr], a fraction of X-cells is replaced with Y-cells, whose ratio is defined as the magnitude of heat-shock, corresponding to the heat-shock period in the experiments (discussed in the following S2.2.1). Then X-cells follows the birth process, and Y-cells the birth-death process. In the death process of Y-cells, the third term of right hand of Eq.(S4) is, for example, approximated as follows:

$$b_y \Delta t \cdot y(t)^{\frac{D}{2}} \simeq b_y \Delta t \cdot \mathrm{floor}\left(y(t)^{\frac{D}{2}}\right) + b_y \mathrm{frac}\left(y(t)^{\frac{D}{2}}\right) \Delta t \cdot 1, \tag{S6}$$

where the functions floor$(\cdot)$ and frac$(\cdot)$ calcurate integer part and fractional (decimal) part, respectively.

Figure S3 shows simulation results of the above process (thin curves) compared with deterministic one (thick curves). Only when weak heat-chock was applied (Fig. S3 **A** and **B**), X-cell group becomes a winner, and in the other cases, X-cell group become a loser (Fig. S3 **C**–**H**). Note that, in the latter cases, the time courses of relative clone size shows once heading for winner site (the value approaching 0 %) and later approaches loser site (the value approaching 100 %) (Fig. S3 **D**, **F**, and **H**). The fate predicted by the stochastic model in the above condition is nothing more than the result by the deterministic model except for the trace fluctuation caused by the stochastic effect in the cell birth-death process. On the contrary, the experimental results fluctuate more widely and the fate are sometimes directed against the prediction by the deterministic model. Therefore the effect of variances observed in the experimental systems was additionally considered as described in the following subsections.

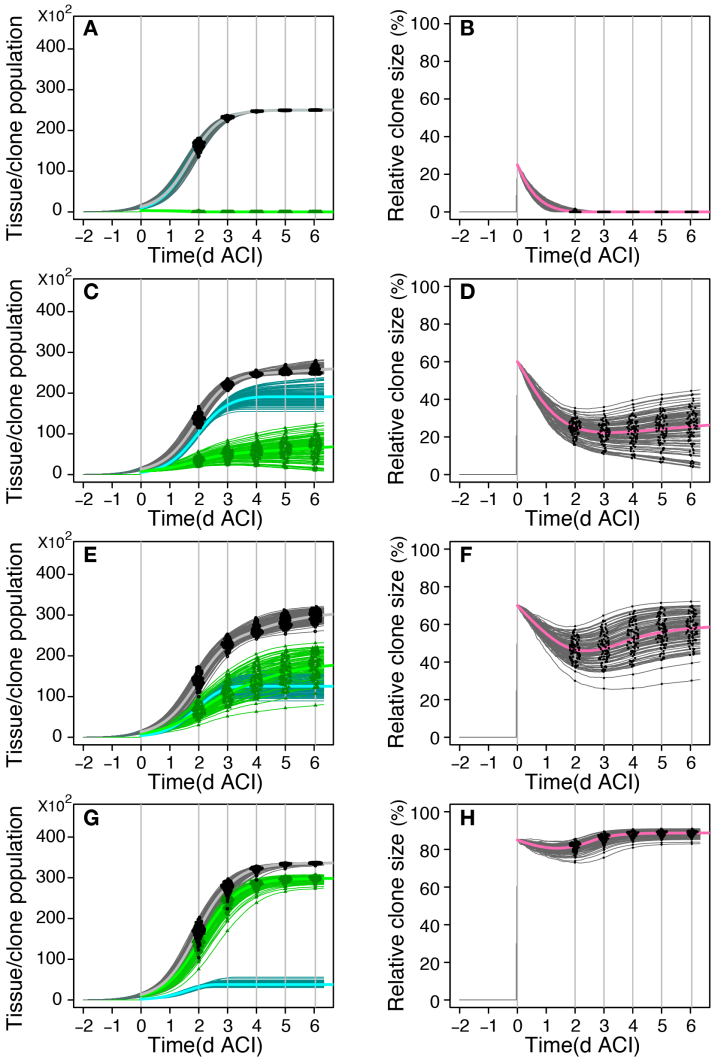

Figure S3: Time evolution of stochastic model for cell competition of Eq (S4) considering cell division and cell death process. The numerical trials were starting from at a point (x_0, y_0)= (30, 0) at time $t = -2$ (d ACI), and various magnitude of heat-shocks were applied at time $t = 0$ (d ACI). The magnitudes of heat-shock were 0.25 (**A** and **B**), 0.60 (**C** and **D**), 0.70 (**E** and **F**), and 0.80 (**G** and **H**), respectively. The traces in **A, C, E** and **G** represent tissue size ($x + y$ denoted by gray), WT domain size (x denoted by cyan), and mutant clone size (y denoted by green). The traces in **B, D, F** and **H** represent relative clone size $y/(x + y)$. Thick and thin lines are the results of deterministic and stochastic models, respectively. The distribution plots (known as 'SinaPlots' [4]) are superimposed: black and green plots in **A**, **C**, **E** and **G** are for, respectively, tissue size and clone size at every observation time corresponding to the experiment; black plots in **A**, **C**, **E** and **G** are for relative clone size. One-hundred trials were performed.

S2.2 Effect of variances

S2.2.1 Fluctuation in efficiency of heat-shock application

Figure S4 shows the heat-shock effect depending on its period, represented using clone size ratio, which was estimated as the ratio of clone size against tissue size using the data obtained from control condition (WT clones). Each plot represents the mean of the data consisting of a mixture of data samples at all observation times (2–6 d ACI), because the ratios were almost constant irrespective of the observation time. The formula of a fitting curve is represented with the relation (clone size ratio) $= a(T/b)^m/\left(1+(T/b)^m\right)$, where T is heat shock period. The parameters were estimated as $a = 0.87$, $b = 15.23$, and $m = 2.30$, using nonlinear regression. Error bars denote standard deviations, whose magnitudes are almost ± 0.1. Therefore in the simulations of Fig. 2 in the main text, the magnitudes of heat-shocks, 0.25, 0.60, 0.70, and 0.85 with 10%-deviation, were respectively adopted for 10-, 20-, 30-, and 60-min-period heat-shocks in the experiment.

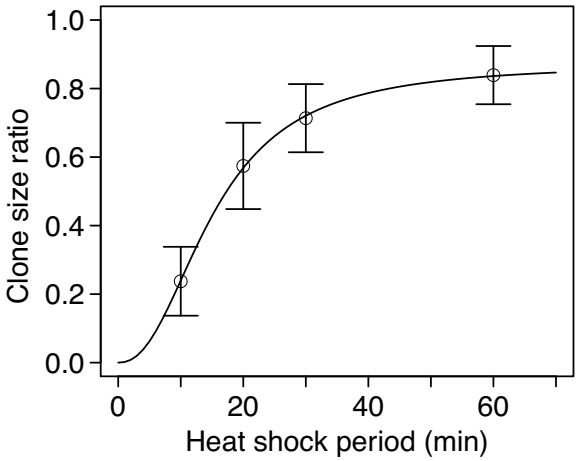

Figure S4: Heat shock period controlling magnitude of mutant clone size.

S2.2.2 Effect of variance in final tissue size.

The variances in tissue size were estimated as the ratio of the standard deviations to the mean value of tissue size as shown in Fig. S5. The variance was as wide as around 30% of tissue size at day 2 but finally reduced to around 10%. The decrease tendency in variance can be caused by stochastic effect of cell division, whose example is seen in the distribuion plots of the tissue size when X-cell group become a winner as shown in Fig. S3**A**. In the simulations of Fig. 2 in the main text, 10%-deviation in carrying capacities, K_x and K_y, were adopted.

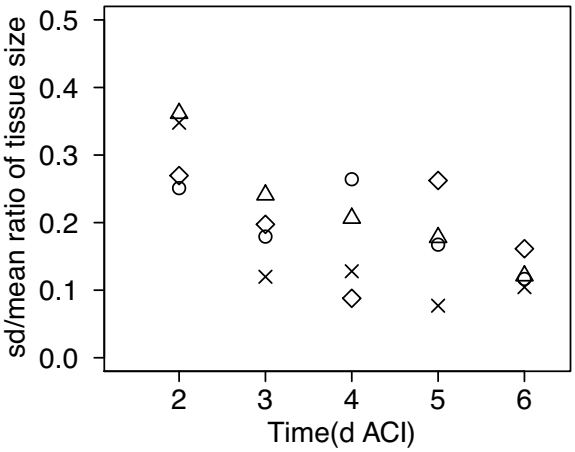

Figure S5: Variance of tissue size depending on observation time. Circles, triangles, crosses, and diamonds represent the values of WT clone-samples, introduced 10-, 20-, 30-, and 60-minutes-period of heat shock, respectively.

S3 Phase portrats in experiment and simulation of stochastic model.

Figure S6 shows phase portraits on the plain of WT domain size and mutant clone domain size redrawn from experimental results (**A**,**C**, **E**, and **G**), and on x–y plane obtained from Monte Carlo simulations of the stochastic model (**B**,**D**, **F**, and **H**). In two extreme case in which heat-shock was weakly or strongly introduced, the fate of the system is clear; WT-cell group becomes a winner in Fig. S6**A** and **B**; On the contrary, it becomes a loser in Fig. S6**G** and **H**. The phase portraits of Fig. S6**C** and **E** are scattered more than the other cases in the experimental results. This could result from the fact that time courses of the solutions are fluctuated around the separatrix (see S1) of the system, which is captured in the simulations of the stochastic model considering the variations in heat-shocks and final tissue size as shown in Fig. S6**D** and **F**.

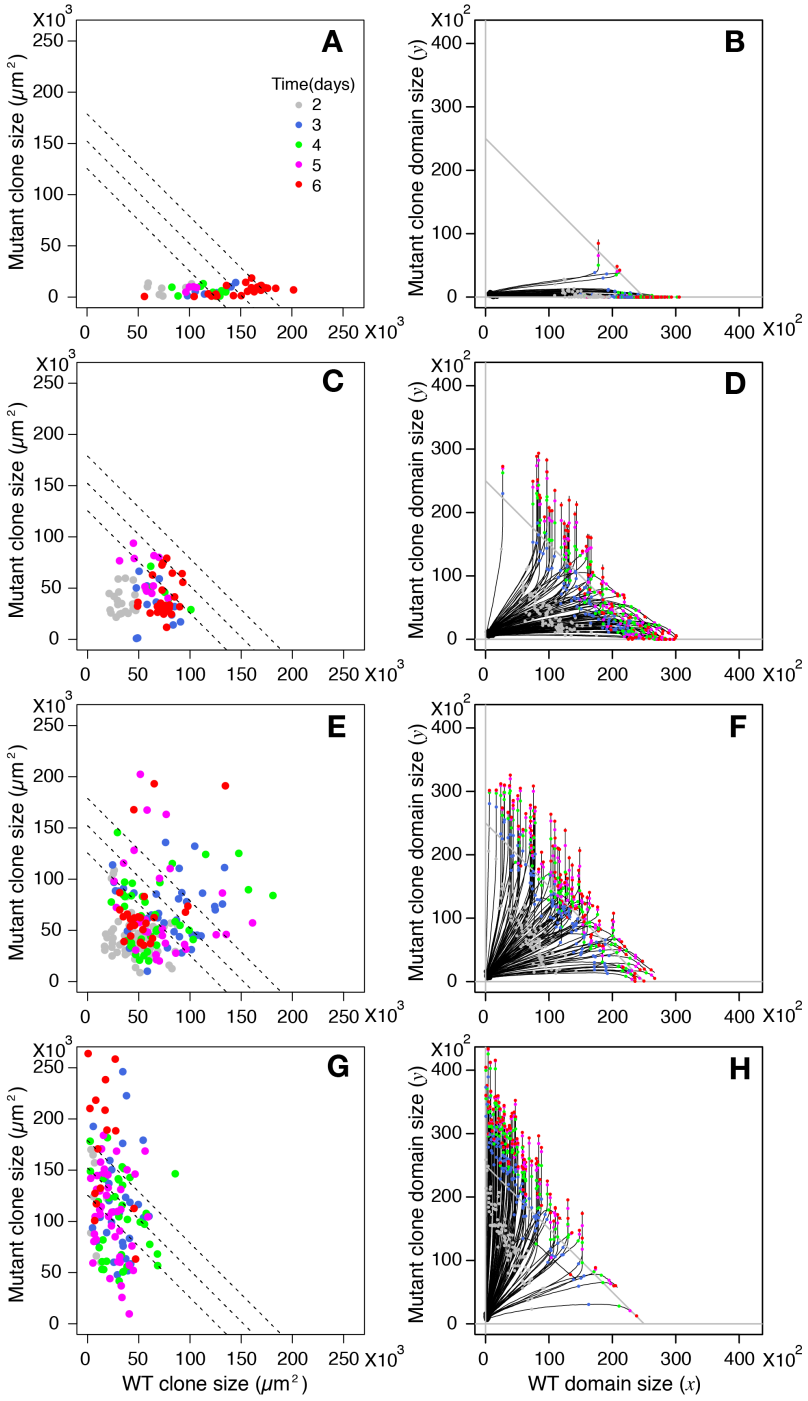

Figure S6: Phase portraits. **A**, **C**, **E**, and **G** Experimental results. **B**, **D**, **F**, and **H** Results of Monte-Carlo simulation using stochastic model. The periods of heat-shock were 10 (**A**), 20 (**C**), 30 (**E**), and 60 [min] (**G**). The magnitudes of heat-shock were 0.25 (**B**), 0.60 (**D**), 0.70 (**F**), and 0.80 (**H**).

S4 Model extension for overgrowth

The tissue size exhibits logistic type growth: exponential growth first and saturation later, whether WT-cell group become winner or not (Fig. S7**A** and **B**). The tissue dominantly composed of mutant cells, however, grows over the saturated size abruptly at later stage (6d ACI) in the experimental results as seen in Fig. 1**M** of the main text. This implies that there is a mechanism activating the proliferation of mutant cells strongly when a certain condition is satisfied. Candidate for the condition is time-dependent or clone-size-dependent mechanism. Figure S7 shows the examples testing these ideas: time-dependent switch (Fig. S7**C** and **D**) and clone-size-dependent switch (Fig. S7**E** and **F**). The carrying capacity of mutant cells K_y was replaced with $1.2K_y$ after $t = 5$(days) in the first example, and when $y > 0.9 \cdot Ky$ in the second example. Because Yki activity is induced specifically at 5d ACI and is required for overgrowth (Fig. S8), the time-dependent mechanism would be promising.

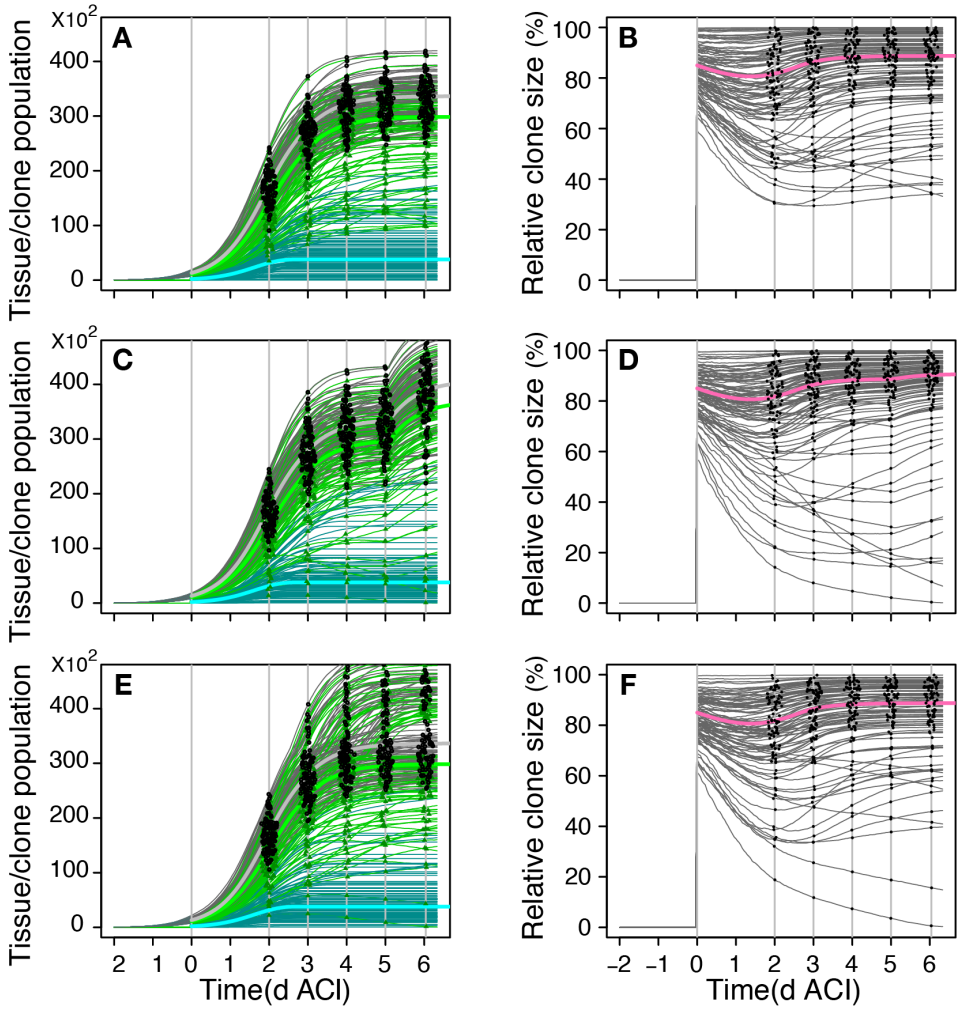

Figure S7: Simulation of over growth. **A** and **B** The model without over growth. **C** and **D** Over growth effect was introduced at time 5 (days). **E** and **F** Over growth effect was introduced when mutant clone size exceeds 90 % of its target size K_y. **A**, **C**, and **E** Time evolution of tissue or clone size. **B**, **D**, and **F** Time evolution of relative clone size against tissue size. Notations are the same as those of Fig. 2 of main text.

References

[1] S. Nishikawa, A. Takamatsu, S. Ohsawa, and T. Igaki,"Mathematical model for cell competition–Predato-prey interactions at the interface between two groups of cells in monolayer tissue," *J. Theor. Biol.*, **404**, 40–50, 2016.

[2] J.D. Murray, 2002, Mathematical Biology I: An Introduction, vol. 17 of Inter- disciplinary Applied Mathematics.

[3] Ballesteros-Arias, L., Saavedra, V., Morata, G., 2014. Cell competition may function either as tumour-suppressing or as tumour-stimulating factor in drosophila. Oncogene 33, 4377-4384.

[4] N. Sidiropoulos, S. H. Sohi, T. L. Pedersen, B. T. Porse, O. Winther, N. Rapin, and F. O. Bagger, "SinaPlot: An Enhanced Chart for Simple and Truthful Representation of Single Observations Over Multiple Classes," Journal of Computational and Graphical Statistics, vol. 44, pp. 1-4, Aug. 2017.

Fig. S8

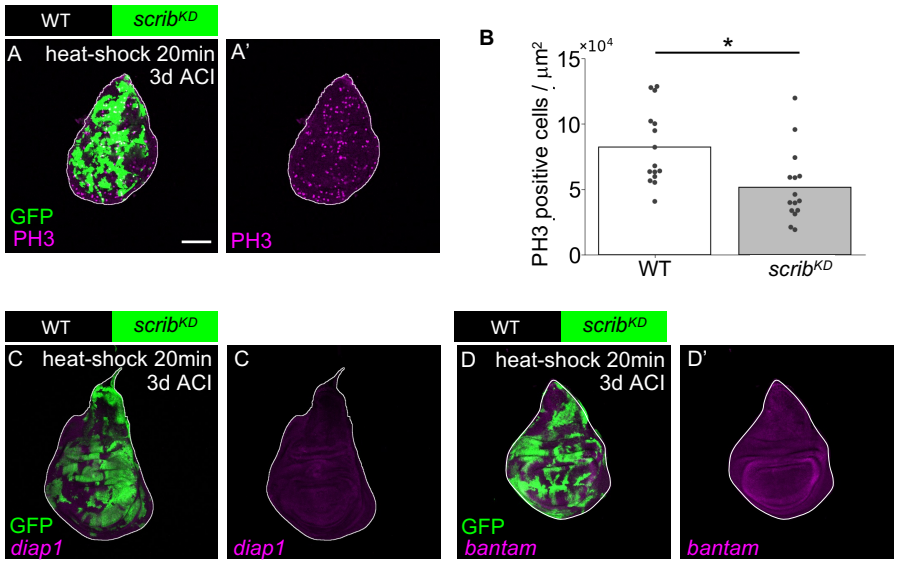

Figure S8 Large *scrib*^{KD} clones overgrow by elevating Yki activity over time.
(A and B) Wing discs bearing GFP-labelled *scrib*^{KD} (C) clones induced by heat-shock for 20min were stained with anti-P-histone H3 (PH3) antibody. PH3-positive cells were quantified both within GFP-positive *scrib*^{KD} clones and in adjacent GFP-negative wild-type regions in the same disc. Quantification was performed using custom Python scripts (B) (n = 15 discs). Paired Student t-test; * $p < 0.05$. Values are means.
(C and D) 3d ACI *DIAP1-LacZ*/+ (C) or *bantam-LacZ*/+ (D) wing discs bearing GFP-labelled *scrib*^{KD} induced by heat-shock for 20min were stained with anti-b-galactosidase antibody.